J Mater Sci (2008) 43:4119–4126
DOI 10.1007/s10853-007-2224-3

REES RAWLINGS FESTSCHRIFT

Polymer-derived microcellular SiOC foams with magnetic functionality

Lisa Biasetto · Adel Francis · Petru Palade · Giovanni Principi · Paolo Colombo

Received: 12 June 2007 / Accepted: 10 October 2007 / Published online: 3 April 2008

Abstract SiOC microcellular ceramic foams possessing soft-ferromagnetic properties were produced from a pre-ceramic polymer, poly-methyl-methacrylate microbeads (PMMA) (used as sacrificial pore formers) and iron silicide micro-powders (as functional filler). The interactions between the matrix and the filler were studied as a function of the amount of powders introduced and the pyrolysis temperature. Magnetic and mechanical properties were also investigated.

Introduction

Si-based pre-ceramic polymers (polysilane, polysiloxanes, polycarbosilane, polysilazanes) have gained increasing interest as precursors for ceramic materials possessing improved and novel properties compared to conventional ceramics. These include resistance to very harsh environments [1], absence of steady state creep, viscoelasticity at very high temperature, [2–4] resistance to crystallization and oxidation [5]. The advantages in using these polymers as ceramic precursors concern both processing (easy shaping, low firing temperatures) and the final material composition and properties. By varying the polymer composition and architecture it is possible to obtain, after crosslinking and pyrolysis (800–1,200 °C, Nitrogen or Argon atmosphere), various ceramic compositions (SiC, SiOC, Si_3N_4, SiCN, SiEOC, SiECN, where E = Al, B, Ti, …) possessing different structures at the nano- and micrometer-range. On the other hand, since such ceramics derive from the pyrolysis of a polymer containing organic functional groups (–CH_3, –C_6H_5, –CH = CH_2, etc.), their elimination during the polymer-to-ceramic conversion leads to components containing pores and cracks, with a volume shrinkage as high as 70%. Manufacturing of bulk components from pre-ceramic polymers, however, is facilitated when the polymer is loaded with a filler powder. Inert filler powders such as Al_2O_3, SiC, B_4C, Si_3N_4, etc., as well as reactive fillers like Ti, Cr, Mo, B, $MoSi_2$, etc., which may react with the solid and gaseous decomposition products of the polymer precursor (and with the heating atmosphere) to form carbides, nitrides, oxides, etc., were successfully used to reduce the polymer-to-ceramic shrinkage and to improve the mechanical properties of non-oxide as well as oxide based polymer-derived ceramics [6–8]. Pyrolysis temperature and atmosphere affect the composition of the resulting filler-loaded ceramics [9].

One further advantage of using fillers in conjunction with pre-ceramic polymers is the possibility to tailor functional properties of the final ceramic materials. For instance, adding filler materials with a high electrical conductivity such as metals or intermetallics offers the possibility of creating polymer-derived ceramic composite materials with low resistivity. Polysiloxanes loaded with 40–50 vol. % of $MoSi_2$ filler powder have been shown to possess an electrical resistivity lower than $10^{-2}\Omega$·m after pyrolysis at temperatures above 1,000 °C [10, 11]. Saha

L. Biasetto (✉) · P. Palade · G. Principi · P. Colombo
Dipartimento di Ingegneria Meccanica-Settore Materiali, Università di Padova, Via Marzolo 9, 35131 Padova, Italy
e-mail: lisa.biasetto@lnl.infn.it

A. Francis
Central Metallurgical Research and Development Institute, CMRDI, Helwan, 87, Cairo, Egypt

P. Colombo
Department of Materials Science and Engineering, The Pennsylvania State University, University Park, PA 16802, USA

et al. [12] prepared polymer-derived SiCN–Fe composites by mixing a liquid ceramic precursor and Fe_3O_4 particles and then reducing iron oxide to α-iron during pyrolysis, producing soft-ferromagnetic ceramics. One further route to functionalize polymer-derived ceramics consists in the embedding transition metals or other elements into silicon oxycarbides [13, 14]. Kolar et al. [15], for instance, recently prepared Si(Co)OC glasses by pyrolysis of a mixture of commercially available poly[methyl(phenyl)] siloxane and Co-phtalate. These shaped ceramics with tunable magnetic properties may find use as protective coatings, magnetic recording media and antistatic shielding [16], thus opening new fields of technological applications within information technology, automotive, electronic, instrumentation, and space engineering.

Pre-ceramic polymers have also been extensively used in the fabrication of ceramic foams. The replica of a highly interconnected foam (i.e., polyurethane) [17], direct foaming [18, 19], and the use of sacrificial fillers [20–22], are the techniques currently used to produce macro and microcellular, open and closed-cells, polymer-derived ceramic foams of various compositions (SiC, SiOC, $3Al_2O_3{\cdot}2SiO_2$ [23], and $2MgO{\cdot}2Al_2O_3{\cdot}5SiO_2$ [24], SiC–TiC [25], SiC–Si_3N_4 [26]). The high versatility of pre-ceramic polymers allows for the production of a wide range of morphologies and compositions, possessing improved mechanical properties compared to ceramic foams synthesized with traditional sintering techniques, due to the presence of dense ceramic struts [17, 18]. Moreover, new techniques (i.e., the nucleation of pores by inducing a thermodynamic instability, borrowing from the plastics literature) [27] have been recently employed to produce pre-ceramic polymer-derived ceramic foams.

Macro and microcellular ceramic foams can find application as molten-metal filters, in fluid separation processes, in aeration of liquids, as adsorbents, as hypervelocity impact shields, as host for interpenetrating composites, in thermal protection systems, etc. [28]. Moreover, through the addiction of low resistivity fillers (in enough quantity to overcome the percolation threshold) they can find application as induction heating elements, radar active materials for stealth components or electromagnetic filters. Colombo et al. [29] recently reported on the electrical functionalization of SiOC macrocellular ceramic foams by addiction of $MoSi_2$, α-SiC, graphite, copper acetate, and Cu_2O. Such lightweight refractory functional materials, which possess specific electromagnetic properties, could find use in several applications, such as regenerable absorbers or regenerable diesel particulate traps.

Up to now, no reports in the literature can be found for magnetic functionalization in ceramic foams produced from pre-ceramic polymers. In the present work we report on the production of magnetic microcellular SiOC foams by the addition of iron silicide powders.

Experimental

SiOC microcellular ceramic magnetic foams were prepared using a commercially available polysiloxane (MK, Waker Chemie, Burgausen, Germany) with a structure comprised of Si–O bonds with –OH and $–CH_3$ substituting groups (denominated as Pre-ceramic Polymer, PP, in the following). The PP was dry mixed with iron silicide (IS) micro-sized powders (Iron Silicide Type 1, Steward Advanced Materials, Chattanooga, TN, average diameter 9 μm) and Poly-methyl-methacrylate microbeads (PMMA) with 25 μm nominal size (Altuglas BS, Altuglas International, Arkema Group, Rho (MI), Italy), by ball-milling for 1 h at room temperature. The mixture was then warm-pressed at 130 °C, 15 MPa for 15 min and then rapidly cooled for 5 min. No cross-linking catalyst was used, as the warm-pressing step fulfilled the double purpose of shaping the powders into the final sample (through melting of the silicone resin) and of thermally cross-linking the PP. After warm-pressing the samples were heat treated in air at 300 °C for 2 h at a heating rate of 0.5 °C/min in order to burnout the PMMA sacrificial template microbeads. By this route, pre-ceramic microcellular foams were obtained [30]. The polymer to ceramic conversion was realized by heating under nitrogen flow up to 1,200 °C for 2 h at a rate 2 °C/min, producing porous ceramic disks of 32 mm diameter and 5.5 mm thickness.

In Table 1 an overview of the prepared samples is reported. The sample labeled S100 is constituted of the as received IS powders. Samples S10010 and S10012 are constituted by the as received IS powders heat treated under nitrogen flow at 1,000 °C and 1,200 °C, respectively. Sample labeled as S40300 was prepared by mixing 40 wt.% of IS and 60 wt.% of PP, powders were ball-milled for 20 min and then heat treated in air at 300 °C (heating rate 2 °C/mmin, 120 min). Concerning samples S3012, S4010, S4012, S5012, and S6012, the weight ratio between PMMA and PP + IS was kept constant at 80–20. The IS weight percentage in the table refers to the PP and IS total amount (i.e., sample labeled S3012 is 30 wt% IS, 70 wt% PP, pyrolyzed at 1,200 °C).

TGA–DTA analysis (10 °C/min from room temperature to 1,210 °C, nitrogen flow, STA 410 NETZSCH-Gerätebau GmbH, Selb, Germany) were performed on the as received IS powders (S100) and on IS and PP polymer mixture (S40300) to study the phase transformation occurring during pyrolysis. TGA–DTA analysis of the polymer to ceramic conversion of the MK polymer was previously reported [14]. X-Ray Diffractometry (Philips PW 1710, Cu Kα radiation) was performed in order to detect the phase composition of the as received IS powders and their possible interactions with the SiOC matrix. The structure of the as received IS powders and of the Fe–Si alloys formed

Table 1 Overview of the prepared samples (IS indicates iron silicide wt.%, and PP pre-ceramic polymer wt.%)

Sample	IS wt. %	PP wt.%	Pyrolysis T (°C)
S100	100	0	RT
S10010	100	0	1,000
S10012	100	0	1,200
S40300	40	60	1,200
S3012	30	70	1,200
S4010	40	60	1,000
S4012	40	60	1,200
S5012	50	50	1,200
S6012	60	40	1,200

within the SiOC ceramic matrix were also investigated by Mössbauer Spectroscopy (carried out with a constant acceleration spectrometer, at room temperature, using a ^{57}Co:Rh source). The magnetic hysteresis parameters were measured at room temperature using a vibrating sample magnetometer (VSM—Model 9600-1, LDJ Electronics, Inc., Mich., USA) up to an applied field H = 1.6 Tesla. The operating principle requires testing of the oscillating sample at uniform frequency and displacement while exposing the sample to a magnetic drive field slowly progressing through a pre-programed cycle. The magnetometer operated at room temperature at a frequency of 85 Hz using nickel sphere reference. The samples were desiccated before the analysis. Scanning Electron Microscopy (Stereoscan 120, Cambridge Instruments, Cambridge, UK) was performed to observe the morphology of the foams. Sample shrinkage during processing was calculated by comparing samples size before PMMA burnout and after pyrolysis.

The crushing strength of the foams was measured at room temperature by compression testing, using UTM (Model 1121, Instron Danvers, MA) with a cross-head speed of 0.5 mm/min, on samples of nominal size of 10 × 5×3.5 mm. Each data point represents the average value of five individuals tests.

Results and discussion

The main properties of the IS powders, as reported in the manufacturer's technical data sheet, are shown in Table 2.

DTA–TGA measurements performed on sample S100 (see Fig. 1a) revealed the presence of one exothermic peak at 494 °C, and two endothermic peaks at 1,053 °C and 1,210 °C, respectively. The weight loss was negligible.

In Fig. 2 the XRD diffraction patterns of the as received IS powders and of IS powder after heat treatment up to 1,000 °C and 1,200 °C under nitrogen flow (heating rate 10 °C/min, dwelling time 10 min) are shown. The as

Table 2 Technical data sheet for the iron silicide powders

SSA (m^2/g)	0.45
M_s (emu/g)	84
True density (g/cm^3)	6.08
Moisture (%)	0.03
Average dimension (μm)	9 ± 5

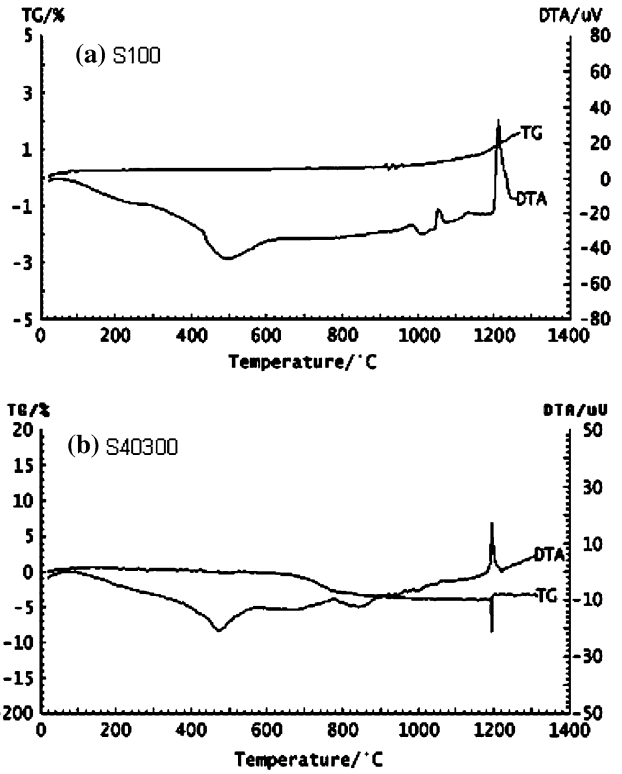

Fig. 1 TGA/DTA patterns for: (**a**) sample S100, and (**b**) sample S40300

received IS powders were confirmed to be $Fe_{1-x}Si_x$ ($0.25 < x < 0.50$) alloys. Inside this compositional range, three main phases were detected: FeSi, Fe_5Si_3, and Fe_3Si.

The FeSi phase, Si 50 at.%, is a narrow-gap non-magnetic semiconductor [31, 32]. The bulk stable iron-monosilicide has a simple cubic Bravais lattice with four Fe atoms and four Si atoms in unit cell with the lattice constant $a = 0.4493$ nm [33]. The DO_3 cubic symmetry (typical for Fe_3Si structure) can be obtained for Si content up to Si 34% although traces of Fe_5Si_3 can also be generally detected [34]. The Fe_3Si cubic structure can be decomposed in two elementary cubic sub-networks made up of BCC and CsCl-type sub-cubes, where the main cubic sites are entirely occupied by iron and the other sub-cubic sites are occupied by both iron and silicon acting as substitutional atoms [35]. The typical symmetry for Fe_5Si_3 is hexagonal. As it can be observed in Fig. 2, after heating the pure IS powder at 1,000 °C the metastable FeSi phase was converted to the Fe_5Si_3 and Fe_3Si phases. The

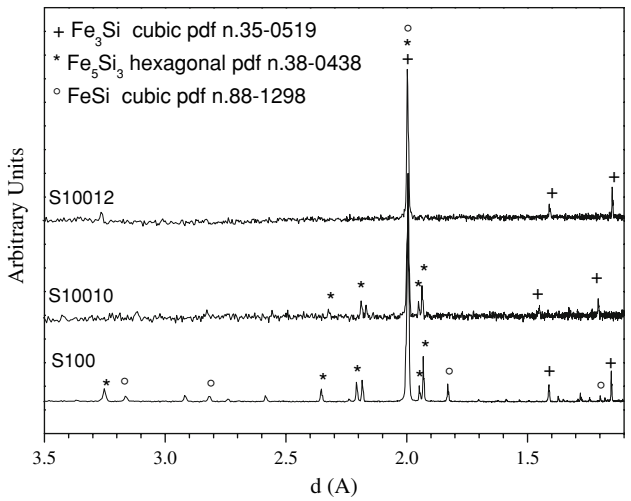

Fig. 2 XRD patterns for pure IS powders as function of heat treatment temperature. S100 (as received IS powders), S10010 (IS heat treated to 1,060 °C under N_2 flow), S10012 (IS powders heat treated to 1,210 °C under N_2 flow)

peak at 494 °C present in the DTA pattern can be attributed to the first phase transformation. After heating to 1,200 °C, the only phase detected was the cubic Fe_3Si structure. The endothermic peak at 1,053 °C in the DTA pattern can thus be attributed to the transformation of the Fe_5Si_3 phase into the Fe_3Si cubic structure. The high-intensity endothermic peak from DTA at 1,200 °C is due to the melting of the Fe_3Si phase [36].

Table 3 reports the measured magnetic parameters of the as received powders and after heating at the above-mentioned temperatures.

As can be observed from Table 3, no definite relationship between annealing temperature and H_c values can be extrapolated. The decrease of H_c with increase of temperature might be due to the reduction of the anisotropy constant K and B_s with annealing temperature. The minor changes in the magnetic properties of IS powder can be attributed the modification of the average size of the micro(nano)-crystallites with the annealing temperature. The phase transformation occurring in the IS powders upon heating was responsible for the increase of B_s values. The paramagnetic phase (Si 50 at.%) was converted to the ferromagnetic Fe_3Si and Fe_5Si_3 after 1,000 °C, and a second transformation occurred at 1,210 °C. At this temperature the only phase detected was Fe_3Si.

Table 3 Measured magnetic properties of the IS powders. B_s, B_r, H_c are the maximum magnetic saturation, remanence, and coercivity, respectively

Sample	Bs (emu/g)	Br (emu/g)	Hc (Oersted)
S100	10.9	0.05	14.5
S10010	11	0.04	6.5
S10012	11	0.04	8.2

In order to verify the effects and possible interactions of the SiOC matrix with the IS powders during pyrolysis, samples with different amounts of IS were prepared. All the samples appeared homogeneous after pyrolysis and they were attracted by a magnet. DTA–TGA analysis on sample S40300 (see Fig. 1b), revealed an endothermic peak at 470 °C and two exothermic peaks at 767 °C and 1,193 °C, respectively (weight loss 4.10 wt%), corresponding to the phase transformation detected in the pure IS powders. The limited shift of phase transformation temperatures to lower values can be attributed to the influence of the PP and its decomposition products deriving from pyrolysis.

The XRD patterns (Fig. 3) of samples S3012, S4010, S4012, S5012, S6012 show that the only Fe–Si phase detected for samples pyrolyzed at 1,200 °C was the Fe_3Si cubic structure. In samples S5012 and S6012, the shoulder in the main peak can be attributed to the presence of α-Fe in the structure. In order to detect the presence of interfaces between the matrix and the filler, TEM investigations should be performed. However, the experimental results collected in this work lead us to suppose that at least at a macroscopic level, no reaction occurred between matrix and filler.

Mössbauer Spectroscopy performed on samples S3012, S4010, S5012 confirmed these results (see Fig. 4). Sample S3012 contained only disordered Fe_3Si, in which Fe exhibited five different local enviroments, corresponding to 0, 1, 2, 3, 4 Si nearest neighbor atoms for the central Fe with respectivly hyperfine magnetic fields of about 33T, 31T, 29T, 25T, and 20T. Sample S4010 contained 89 wt% disordered Fe_3Si and 11 wt% Fe_5Si_3, as calculated from the relative Mössbauer spectral area (RA). Sample S5012 contained majoritary disordered Fe_3Si (65.1% of RA), Fe–Si–O phases where Fe valence is +2 (31.2% of RA), and some minor Fe–Si–O phase where Fe valence is +3

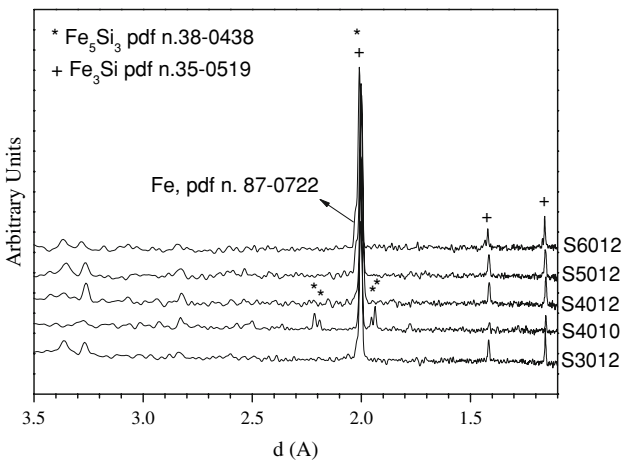

Fig. 3 XRD patterns for SiOC + IS microcellular foams

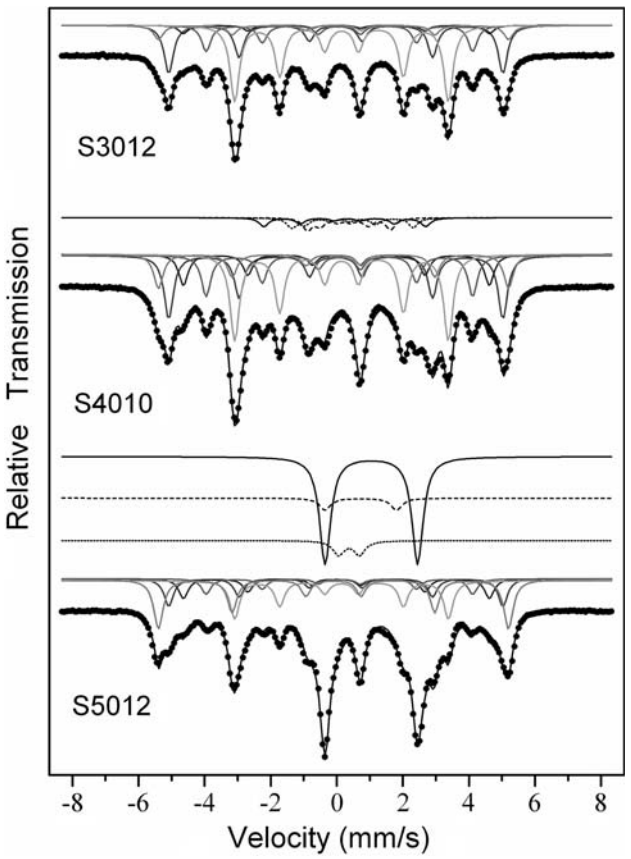

Fig. 4 Comparison of Mössbauer spectra for samples S3012 (IS 30 wt%, 1,200 °C N_2), S4010 (IS 40 wt%, 1,000 °C N_2), and S5012 (IS 50 wt%, 1,200 °C N_2)

(3.5% of RA). In all the samples there were five inequivalent positions, such as those for a disordered Fe–Si solid solution (see Table 4). The higher occupancy of Fe site with 0Si nn in sample S5012 agrees with the XRD indication of the presence of α-Fe in samples with increasing IS content.

Table 5 reports the value for various magnetic parameters of samples S0012, S3012, S4012, S4010, S5012, and S6012, at a moment range equal to 1 emu.

It is well known that the magnetic properties of materials, and in particular of ferrites, are influenced by numerous factors such as cationic composition, microstructure, purity, homogeneity, non-stoichiometry, and particle size [37–39].

In the literature there is no report concerning the preparation and characterization of SiOC ceramics possessing magnetic properties, but Saha et al. recently investigated polymer-derived SiCN materials containing α-Fe [12]. The B_s values indicate that Fe_3Si and Fe_5Si_3 are the predominant magnetic phases at higher temperature. However their values are found to be lower than would have been expected for pure Fe–Si powder. The reason may be due to the mechanical constraint imposed on the Fe–Si particles by the SiOC matrix that restricts domain rotation or to the

Table 4 Magnetic parameters from Mössbauer measurements: nn, nearest neighbors; HF, hyperfine magnetic field

Sample	Si nn for Fe	HF (T)	Occupancy
S3012	0 Si	32.85	0.08
S4010			0.13
S5012			0.32
S3012	1 Si	31.35	0.28
S4010			0.25
S5012			0.18
S3012	2 Si	28.70	0.05
S4010			0.12
S5012			0.13
S3012	3 Si	25.01	0.15
S4010			0.16
S5012			0.11
S3012	4 Si	20.04	0.44
S4010			0.34
S5012			0.26

interfaces between the particles and the matrix that pin the magnetization and therefore resist the rotation and motion of the magnetic domain, as suggested for a very similar system by Saha et al. [12]. Residual stress measurements would need to be performed in order to prove conclusively this speculation. Generally, a pore in a magnetic material affects the permeability via the decrease in magnetization per unit volume and moreover via the increase in the demagnetizing field. The two above factors may act together to lower the magnetization of the ceramic composite. However more detailed investigations are necessary in order to understand in details the dependence between microstructure, the magnetization processes and the percentage of porosity.

The variation in the coercive force can be attributed to the variation of the multidomain (MD) structure of the iron silicides, where the B_r/B_s increased to 0.0126 for the heat-treated S50 sample at 1,200 °C. When the IS wt.% increases in the samples, the saturation magnetization decreases, probably due to imperfections in the solid. The presence of pores, interfacial and surface defects, structural defects such as particles of a non-magnetic phase in the magnetic material may restrict the motion of domain walls.

Saturation magnetization (B_s) is a measure of the total amount of magnetic material in the sample, while the coercivity, H_c, is a measure of its magnetic stability. The ratio B_r/B_s is commonly used as indicators of domain states and, indirectly, grain size. High values of B_r/B_s (>0.5) indicate small (<0.1 μm or so) single-domain (SD) grains, and low values (<0.1) are characteristic of large (>15–20 μm) MD grains [40–42]. Magnetic properties depend on the microscopic and macroscopic structure (crystal grain structure,

Table 5 Magnetization parameters measured by VSM

Sample	IS wt% after pyrolysis	B_s (emu/g)	B_s^{IS} (emu/g)	B_r (emu/g)	H_c (Oersted)	B_r/B_s
S0012	–	0.03	–	0.004	10.6	0.166
S3012	33.5	12.1	36.2	0.05	4.0	0.004
S4012	43.9	11.6	26.5	0.05	16.2	0.004
S4010	43.9	10.5	23.9	0.05	7.9	0.005
S5012	54.05	9.5	17.5	0.12	11.4	0.013
S6012	63.8	17.0	26.7	0.06	8.8	0.004

B_s is the magnetic induction of the measured sample, B_s^{IS} is the recalculated value (as a function of the IS wt% after pyrolysis), B_r is the remaining induction magnetization, H_c the coercive force, and B_r/B_s the remanence ratio

grain boundaries). The microstructure of the solid controls the wanted or unwanted movement of magnetic domain boundaries and therefore affects the possibility of magnetic (re-) ordering processes and the degree of magnetization. Since the measurement of the magnetization depends on the investigated amount of material, one has to relate the magnetization to the mass or the volume of the sample.

In order to reveal the nature of the domain states existing in our system, we can summarize as follows the data related to compositional and thermal variation of the hysteresis parameters (see Fig. 5): (1) the hysteresis loops of all the compositions investigated are very narrow; (2) the shape of the loop does not change appreciably with temperature 1,000 and 1,200 °C; (3) the remanence ratio B_r/B_s of all the compositions is less than 0.01 and does not vary with temperature, and 4) the coercivity is small and almost temperature independent but depends on the IS content. All of the above observations support the presence of M-D grains, and hence we conclude that all the compositions investigated by us contain M-D grains in predominance. The fact that the IS filler does not react with the pre-ceramic polymer matrix during pyrolysis is positive as it allows the functional powder to maintain and manifest its properties in the final porous ceramic component.

In Fig. 6, Scanning Electron Microscope images of IS as received powders and of SiOC foam samples are shown. For comparison, an image of a pure SiOC foam without IS fillers has been shown as well (Fig. 6b). All the foams in the figure were pyrolyzed at 1,200 °C in nitrogen, and contained different amounts of iron silicide powders (0 (Fig. 6b), 40 (Fig. 6c), and 60 (Fig. 6d) wt%). IS particles can be seen to be present in the cell walls and inside the struts of the foams (see especially fig 6c; the particles were identified as containing Fe by EDX). As it can be observed in Fig. 6a and c, IS particles possess a smaller size in comparison to the as received powders (the average dimension changed from about nine microns—which correspond roughly to the cell size of the ceramic foam—to less than a micron after processing at 1,200 °C). This size reduction can be related to the fact that, during pyrolysis at

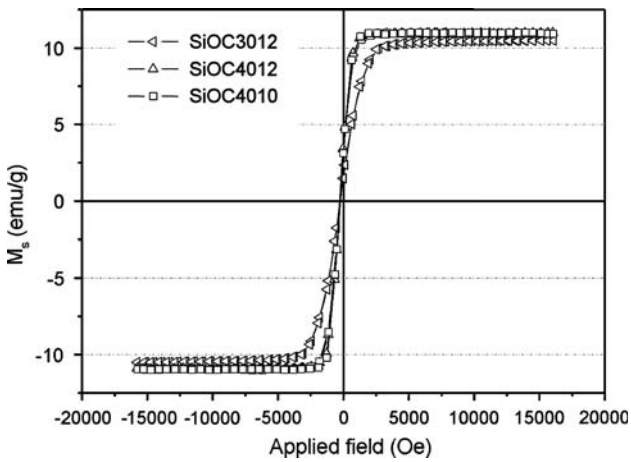

Fig. 5 Typical magnetization curves of the prepared samples (up to 16,000 Oe)

1,200 °C, the IS particles melt (see DTA data), thus resulting in new Fe_3Si particles uniformly dispersed inside the matrix. The foam morphology was affected by the presence of magnetic particles, resulting in samples with a much less regular porosity with increasing amount of iron silicide filler. This effect is related to the change due to the presence of a high amount of filler particles in the rheological behavior of the pre-ceramic polymer, which had an increased viscosity in the warm-pressing forming stage. However, well defined cellwalls and struts could still be observed in the S6012 sample, in spite of the high IS powder content (see Fig. 6d).

As expected, the relative density value increased with increasing amount of iron silicide, while the shrinkage decreased due to the presence of the inert filler. Compression strength values, see Table 6, decreased with increasing IS wt%, certainly due to the disruption of the porous macrostructure with an associate increase of defects within the ceramic struts. The strength values, however, were quite high considering the fact that the samples have a porosity > 70 vol%.

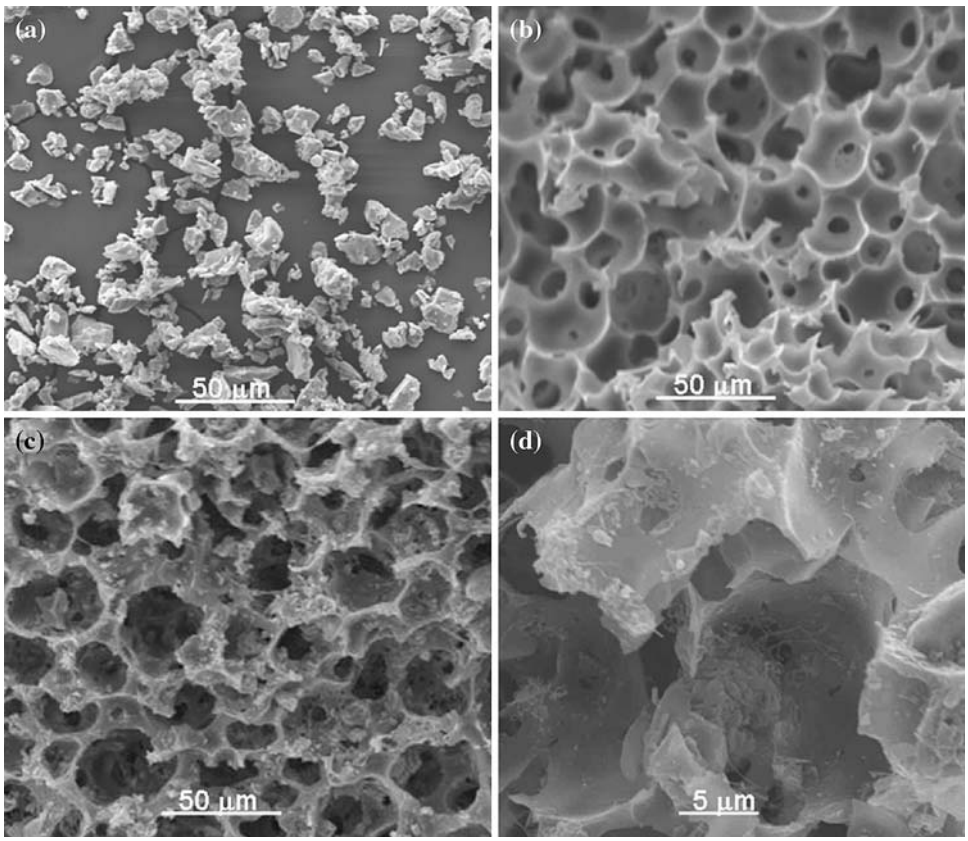

Fig. 6 SEM pictures of: (**a**) as received IS powders; (**b**) S0012 (pure SiOC foam, 0 wt% IS, 1,200 °C, N_2); (**c**) S4012 (40 wt% IS, 1,200 °C, N_2); (**d**) S6012 (60 wt% IS, 1,200 °C, N_2)

Table 6 Density (ρ), volumetric shrinkage upon pyrolysis, and compression strength (σ) of the various samples

Sample	ρ (g/cm^3)	ΔV % (shrinkage)	σ (MPa)
S0012	0.26 ± 0.01	64.4	9 ± 0.3
S3012	0.37 ± 0.01	42.2	2.2 ± 0.3
S4012	0.39 ± 0.01	41.5	3.1 ± 0.3
S5012	0.42 ± 0.01	41.0	1.8 ± 0.2
S6012	0.45 ± 0.01	39.5	1.3 ± 0.2

S0012 refers to a SiOC microcellular foam (containing no fillers, produced using PMMA 25 µm as sacrificial template and pyrolyzed at 1,200 °C)

Conclusions

Ceramic foams possessing magnetic functionalization were produced from a pre-ceramic polymer and iron silicide filler. Iron silicide powders were subjected to phase transformation and melting during pyrolysis, leading to a final iron silicide phase consisting of fine cubic Fe_3Si particles embedded in the SiOC ceramic matrix. Microstructural characterization by means of Mössbauer Spectrometry and X-Ray Diffractometer indicated that no significant reaction occurred between the SiOC matrix and the iron silicide filler. With increasing iron silicide content, the magnetic response was proportionally increased. The magnetic parameters such as H_c and B_r/B_s revealed the presence of a multi domain grain structure, thus affecting the magnetic response of the composite material. The foam morphology became more inhomogeneous and the compression strength decreased with increasing the iron silicide amount in the starting mixture. The proposed processing procedure allowed to prepare soft-ferromagnetic SiOC microcellular foams, possessing a reasonable compression strength (1.3–3.1 MPa) and a saturation magnetization in the range 9.5–17 emu/g, depending on the amount of fillers introduced.

Acknowledgements This research was supported by EC, FP6 through MCRTN-CT-019601, "PolyCerNet". Travel funding from the Protocol of Scientific and Technological Co-operation between Italy and Egypt (2004–2006), project No.13 NMat2 (New materials and ecologically sustainable technologies) titled " Preparation and Properties of Nanocomposites SiON- and SiOC-Based Ceramic Materials" is gratefully acknowledged.

References

1. Sorarù GD, Modena S, Guadagnino E, Colombo P (2002) J Am Ceram Soc 85:1529
2. Rouxel T, Sorarù GD, Vicens J (2001) J Am Ceram Soc 84:1052
3. Rouxel T, Massouras G, Sorarù GD (1999) J Sol-gel Sci Tech 14:87
4. Scarmi A, Sorarù GD, Raj R (2005) J Non-Cryst Solids 351:2238
5. Chollon G, Aldacourrou B, Capes L (1998) J Mater Sci 33:901. doi:10.1023/A:1004395308173

6. Greil P (1995) J Am Ceram Soc 78:835
7. Seyferth D, Bryson N, Workman DP, Sobon CA (1991) J Am Ceram Soc 74:2687
8. Suttor D, Kleebe H-J, Ziegler G (1997) J Am Ceram Soc 80:2541
9. Wei Q, Pippel E, Woltersdorf J, Scheffler M, Greil P (2002) Mater Chem Phys 73:281
10. Cordelair J (1999) Electrical properties of polymer/filler derived ceramics; Ph.D. Thesis, University of Erlangen-Nuernberg, Erlangen, Germany
11. Bergero L, Sglavo VM, Sorarù GD (2005) J Am Ceram Soc 88:3222
12. Saha A, Shah S, Raj R (2003) J Mater Res 18:2549
13. Sorarù GD, Babonneau F, Maurina S, Vicens J (1998) J Non-Cryst Solids 224:173
14. Harshe R, Balan C, Riedel R (2004) J Eur Ceram Soc 24:3471
15. Kolar F, Machovic V, Svitilova J (2006) J Non-Cryst Solids 352:2892
16. MacLachlan M, Ginzburg M, Coombs NL, Coyle TW, Raju NP, Greedan JE, Ozin GA, Manners I (2000) Science 287:1460
17. Bao X, Nangrejo MR, Edirisinghe MJ (2000) J Mater Sci 35:4365. doi:10.1023/A:1004805023228
18. Colombo P, Hellmann JR (2002) Mat Res Innovat 6:260
19. Zeschky J, Hofner T, Arnold C, Weiβmann R, Bahloul D, Scheaffler M, Greil P (2005) Acta Mater 53:927
20. Kim Y-W, Jin Y-J, Chun Y-S, Song I-H, Kim H-D (2005) Scr Mater 53:921
21. Kim Y-W, Kim S-H, Song I-H, Kim H-D, Park CB (2005) J Am Ceram Soc 88:2949
22. Shibuya A, Takahashi T, Koyama K (2007) Comp Sci Tech 67:119
23. Kim Y-W, Kim H-D, Park CB (2005) J Am Ceram Soc 88:3311
24. Song I-H, Kim M-J, Kim H-D, Kim Y-W (2006) Scr Mater 54:1521
25. Nangrejo MR, Bao X, Edirisinghe MJ (2001) Int J Inorg Mat 3:37
26. Nangrejo MR, Bao X, Edirisinghe MJ (2000) J Europ Ceram Soc 20:1777
27. Kim Y-W, Kim S-H, Xu X, Choi C-H, Park C-B (2002) J Mater Sci Lett 21:1667
28. Scheffler M, Colombo P (eds) (2005) Cellular ceramics: Structure, manufacturing, properties and applications. WILEY-VCH Verlag GmbH, Weinheim, Germany, p 645
29. Colombo P, Gambaryan-Roisman T, Scheffler M, Buhler P, Greil P (2001) J Am Ceram Soc 84:2265
30. Colombo P, Bernardo E, Biasetto L (2004) J Am Ceram Soc 87:152
31. Wertheim GK, Jaccarino V, Wernick JH et al (1965) Phys Lett 18:89
32. Jaccarino V, Wertheim GK, Wernic JH et al (1967) Phys Rev 160:476
33. Watanabe H, Yamamoto H, Ito K (1963) J Phys Soc Jpn 18:995
34. Varga LK, Mazaleyrat F, Kovac J, Greneche JM (2002) J Phys: Condens Matter 14:1985
35. Starke U, Schardt J, Weiss W, Meier W et al (2001) Europhys Lett 56:822
36. Raghavan V (1987) Phase diagram of ternary iron alloys, ASM International, Materials Park
37. Polyakov VV, Egorov A (1995) Powder Metall Met Ceramics 33:9
38. Radomysel'skii ID, Yaglo GI, Efremova NF (1984) Poroshk Metall 1:73
39. James BA, Williams G (1979) Powder Metall 2:75
40. Butler RF, Banerjee SK (1975) J Geoph Res 80:4049
41. Özdemir Ö, Dunlop DJ, Moskowitz BM (2002) Earth Planet Sci Lett 194:343
42. Dunlop DJ (1986) J Geoph Res B 91:9569